

Benchmarking Humanoid Imitation Learning with Motion Difficulty

Zhaorui Meng
Xiamen University
Xiamen, China

mengzhaorui@stu.xmu.edu.cn

Anjun Chen*
Xiamen University
Xiamen, China

anjunchen@xmu.edu.cn

Lu Yin
Xiamen University
Xiamen, China

yinlu@stu.xmu.edu.cn

Shihui Guo
Xiamen University
Xiamen, China

guoshihui@xmu.edu.cn

Xinrui Chen
Xiamen University
Xiamen, China

cxr1112021@163.com

Yipeng Qin
Cardiff University
Cardiff, UK

qiny16@cardiff.ac.uk

Abstract

Physics-based motion imitation is central to humanoid control, yet current evaluation metrics (e.g., joint position error) only measure how well a policy imitates but not how difficult the motion itself is. This conflates policy performance with motion difficulty, obscuring whether failures stem from poor learning or inherently challenging motions. In this work, we address this gap with **Motion Difficulty Score (MDS)**, a novel metric that defines and quantifies imitation difficulty independent of policy performance. Grounded in rigid-body dynamics, MDS interprets difficulty as the torque variation induced by small pose perturbations: larger torque-to-pose variation yields flatter reward landscapes and thus higher learning difficulty. MDS captures this through three properties of the perturbation-induced torque space: volume, variance, and temporal variability. We also use it to construct MD-AMASS, a difficulty-aware repartitioning of the AMASS dataset. Empirically, we rigorously validate MDS by demonstrating its explanatory power on the performance of state-of-the-art motion imitation policies. We further demonstrate the utility of MDS through two new MDS-based metrics: *Maximum Imitable Difficulty (MID)* and *Difficulty-Stratified Joint Error (DSJE)*, providing fresh insights into imitation learning.

1. Introduction

Physics-based motion imitation learning, which generates physically plausible human-like motions, has been widely adopted in humanoid robotics [24–26]. In simulation, imitation learning policies use human motion data as reference inputs to control humanoids to replicate these motions

*Corresponding author.

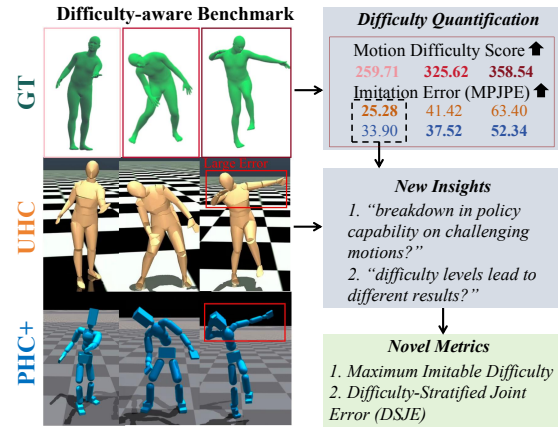


Figure 1. Our Motion Difficulty Score (MDS) accurately quantifies motion difficulty: *higher MDS* \rightarrow *higher error on policies* \rightarrow *harder to imitate*. Beyond validation, MDS reveals nuanced insights into imitation learning: e.g., PHC+ [25] dominates overall but UHC [26] outperforms it on easy motions, challenging a common belief in this field. Leveraging this benchmark, we introduce *Maximum Imitable Difficulty (MID)* and *Difficulty-stratified Joint Error (DSJE)*, enabling fine-grained, difficulty-aware evaluation of imitation learning.

— a critical foundation for real-world robot deployment. This task remains highly challenging as robots can deviate from the reference trajectory and may even fall. Reinforcement learning (RL)-based imitation learning policies have achieved good performance on individual motion sequences, and some approaches (e.g., UHC [26], PHC [24]) have achieved high success rates on large-scale datasets. However, despite the overall high success rates, large errors still occur in reproducing highly challenging motions. Intuitively, a more capable policy is expected to exhibit higher

success rates or lower tracking errors. Nevertheless, imitation performance is not influenced only by the intrinsic capability of the policy itself but also the kinematic and temporal diversity of the target motion. Existing motion datasets [7, 27] offers a large and diverse collection of motions, yet provide no explicit annotations or metrics that quantify imitation difficulty, making it difficult to disentangle policy limitations from the intrinsic difficulty of target motions, obscuring whether performance degradation stems from inadequate learning or intrinsically difficult motions.

However, evaluating the imitation difficulty of a motion is inherently challenging. Empirically, a policy trained using existing imitation learning methods tends to perform better on certain motions than others. For example, a ballet sequence is considerably more challenging than a simple standing pose. But why? Therefore, explicitly defining and quantifying the “imitation difficulty” of a motion remains an open challenge. Establishing such a measure could not only provide a novel benchmarking paradigm for evaluating policy capability in imitation learning but also open new avenues for motion-related research, such as guiding policy training, imitation-friendly motion optimization, and physics-plausible motion restoration.

In this paper, we address the above-mentioned gap by introducing the first explicit definition of the intrinsic imitation difficulty of human motions themselves, and quantify it as a novel **Motion Difficulty Score (MDS)**. We begin by defining the imitation difficulty of a motion from the perspective of rigid-body dynamics. In humanoid control, the motion of a simulated avatar is driven by torques generated by the control policy. For a given motion sequence, the relationship between joint torques τ and motion follows the equations of rigid-body motion [12], implying that a unique torque corresponds to an exact motion. However, when small motion deviations require large torque adjustments, reinforcement learning (and gradient-based optimization) encounters flat or plateau-like reward landscapes: substantial torque changes produce nearly identical poses and thus receive nearly identical rewards. In such regions, the reward signal becomes weakly informative, offering little guidance for effective policy improvement. Intuitively, for an easy motion such as a hand wave, a slight positional change calls for only a mild torque adjustment, allowing the policy to obtain clear, consistent improvement signals. In contrast, for a difficult motion such as a single-leg stance, the reward landscape collapses into a Dirac-delta-like spike, where reward is concentrated in an extremely narrow region and flattens almost immediately outside it. As a result, the policy explores torque updates across the plateau but obtains nearly identical rewards, making the motion substantially harder to learn. Therefore, we define the *imitation difficulty of a motion* S as the torque variation \mathcal{T} induced by a bounded pose error neighborhood, which is characterized by: 1) its vol-

ume, 2) its variance, and 3) its temporal variability. Practically, we compute the Motion Difficulty Score (MDS) as the aggregate of three complementary components corresponding to the factors above: 1) Spectral Diversity, 2) Variance Diversity, and 3) Segment Diversity. Building on MDS, we introduce MD-AMASS, a difficulty-aware repartitioning of the AMASS dataset. Our experiments reveal that MDS not only explains the performance behavior of state-of-the-art imitation policies but also enables new diagnostic analyses through the derived Maximum Imitable Difficulty (MID) and Difficulty-Stratified Joint Error (DSJE) metrics.

In Summary, our contributions include:

- We introduce the first definition of the imitation difficulty of human motions, derived directly from rigid-body dynamics.
- We propose Motion Difficulty Score (MDS), a novel metric that quantifies motion difficulty as the torque variation induced by small pose perturbations, captured through three complementary components: Spectral Diversity, Variance Diversity, and Segment Diversity.
- We construct MD-AMASS, the first difficulty-aware repartitioning of the AMASS dataset, enabling systematic evaluation across varying difficulty levels.
- Extensive experiments show that MDS reliably explains performance trends in state-of-the-art motion imitation policies, validating its effectiveness.
- Moreover, we introduce two MDS-derived metrics: Maximum Imitable Difficulty (MID) and Difficulty-Stratified Joint Error (DSJE), revealing novel insights in imitation learning unattainable without MDS.

2. Related Works

2.1. Physics-based Human Motion Imitation

Physics-based human motion imitation aims to create simulated characters governed by physical laws [5, 9, 11, 14–16, 29, 33–36, 38, 45, 46, 48, 49, 52], enabling the generation of dynamically plausible human behaviors. Due to the well-known generalization challenges in reinforcement learning based controllers, early efforts focused on small-scale tasks, such as interactive control via user input [5, 36, 38, 45] or modular skills like locomotion [34] and dribbling [38]. Recent advances have shifted toward large-scale datasets and multi-sequence imitation. ScaDiver [47] pioneered large-scale imitation of the CMU MoCap dataset [7] using a mixture-of-experts framework, while MoCapAct [44] distilled per-clip experts into a unified policy with minimal performance loss. Most recently, universal motion imitation using a single policy has emerged as a promising direction toward general humanoid control. UHC [26] successfully imitates 97% of the AMASS dataset by introducing residual root forces [51] for balance recovery. Its successor, PHC [24], eliminates all non-physical forces,

achieving superior physical fidelity while preserving high tracking accuracy. Related works also explore reference tracking [8, 9, 31, 33, 37, 47, 52] and object interaction [8, 29] in simulation. However, UHC and PHC stand out for their ability to handle diverse daily motions and interactions without task-specific tuning, demonstrating robust generalization. Despite these advances, existing evaluations and reward designs rely almost exclusively on similarity-to-reference metrics (e.g., joint position error) across heterogeneous motion datasets, overlooking intrinsic motion properties such as dynamic stability and control fragility.

2.2. Human Motion Benchmark

Human motion data serves as a foundational resource for humanoid control, character animation, motion capture, and related applications. In recent years, the widespread adoption of unified parametric models [23, 32] has enabled large-scale datasets to be standardized and broadly applied across motion research. To address limitations in data scale and diversity, recent efforts have turned to internet videos as a rich source for constructing new datasets [6, 10, 22, 42, 56]. Humanoid-X [28] stands out by integrating large-scale video-reconstructed motions with high-fidelity motion capture subsets, creating a hybrid dataset of unprecedented scope. PHMUA [20] aim to enhance physical plausibility. Meanwhile, datasets such as [1, 7, 54] are widely adopted due to their high kinematic accuracy and rich action variety, though constrained by complex camera calibration and marker-based setups. For tasks like general motion imitation and physics-based motion reconstruction, large volumes of uniformly represented data are essential. H36M [19] provides extensive video-captured human motion, while the widely adapted AMASS dataset [27] unifies diverse sources under the SMPL parameterization. The community has also produced specialized datasets: [3, 21, 42] focus on dance by curating motion sequences synchronized with musical beats—a core aspect of expressive human movement, while BMLHandball [17] builds a database of penalty throw actions. These efforts reflect a growing demand for task-specific motion diversity. However, most existing approaches collect data based on semantic categories (e.g., "dance" vs. "locomotion"). While practitioners observe that dance motions are harder to imitate than daily actions, no analysis quantifies the intrinsic difficulty of individual motions, nor explains *why* certain motions are harder. As a result, difficulty-aware applications and in-depth evaluations remain largely unexplored.

3. Motivation and Preliminaries

Physics-based human motion imitation leverages physically simulated environments to drive a torque-controlled avatar in mimicking a reference motion. A central challenge in this process is the avatar’s propensity to deviate from the refer-

ence, often resulting in stumbles or catastrophic falls. To address this, the research community has explored numerous strategies, including RL reward design [34, 38], policy architecture innovation [24, 47], and motion preprocessing [55], all unified by the goal of maximizing similarity to the reference, irrespective of the reference motion itself. Yet, *tracking fidelity is not solely a function of policy capability; it is co-determined by the intrinsic difficulty of the motion*. Empirically, a well-trained policy exhibits striking performance variance across training motions (e.g., joint position error ranging from ~ 16 mm on static T-pose to over 150 mm on dynamic motions such as long jump) despite identical training conditions. Therefore, explicitly quantifying motion difficulty is pivotal: it forms the foundation for fairer policy evaluation, difficulty-aware curriculum learning, and physics-plausible restoration of flawed motions, opening new research frontiers in imitation learning. In this work, we aim to fill this gap by introducing a new metric, orthogonal to motion accuracy, that defines and quantifies motion difficulty.

Problem Setup and Notations. Our approach is grounded in rigid-body dynamics. We adopt the standard human motion imitation setup with a torque-controlled, floating-base humanoid [57] and follow the mass distribution protocol from [40]. We define key relevant 3D human motion properties, including:

- *Joint rotations* (i.e., pose) $\theta \in \mathbb{R}^{3J}$ represented by Euler angles, with their time derivatives $\dot{\theta}$ and $\ddot{\theta}$ representing the angular velocity and angular acceleration, respectively;
- *Global joint positions* $r \in \mathbb{R}^{3J}$ with their time derivatives \dot{r} and \ddot{r} representing the linear velocity and acceleration in the global coordinate system, respectively.

We use $J = 24$ to denote the number of joints in the SMPL model. Furthermore, we have:

- *Character configuration* $q = [r_{\text{root}}, \theta] \in \mathbb{R}^N$ defined by its local pose and global translation, where $r_{\text{root}} \in \mathbb{R}^3$ is global translation of the root joint and $N = 3 + 3J$ is the number of degrees of freedom (DoF). The time derivatives \dot{q} and \ddot{q} represent the generalized velocity and acceleration, respectively.

Equation of Rigid-Body Motion. In rigid-body dynamics, we define the torque vector $\tau \in \mathbb{R}^N$ for the controlled character, where each dimension corresponds to the force applied to the respective degree of freedom. Then, the character configuration q , the torque τ , the generalized velocity \dot{q} and acceleration \ddot{q} , satisfy the following equation [12]:

$$M(q)\ddot{q} + h(q, \dot{q}) = \tau + f_{\text{ext}} \quad (1)$$

where $M \in \mathbb{R}^{N \times N}$ is the inertia matrix; $h \in \mathbb{R}^N$ is the non-linear term accounting for gravity, Coriolis, and centrifugal forces; and f_{ext} denotes the external forces from the surrounding environment of the character.

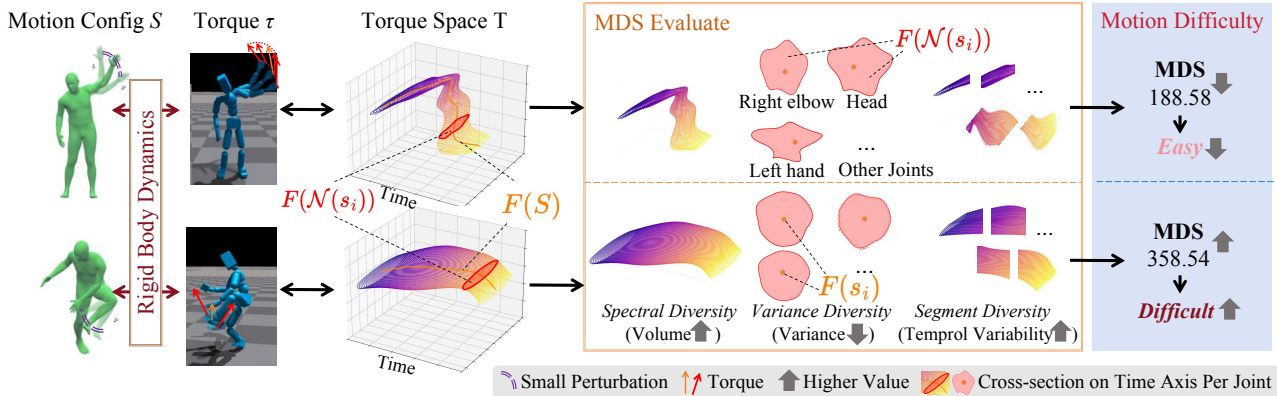


Figure 2. Illustration of MDS: For an *easy* motion (top-left), small pose perturbations induce small torque variance and hence low sensitivity to perturbation, the 1) smaller torque space volume, 2) larger variation across joints (larger volume on the waving hand joints than others) and 3) larger temporal variability makes MDS rates the motion as easier. In contrast, for a *difficult* motion (bottom-left), the same level of perturbation yields large torque variance across all joints, leading to a high MDS.

4. The MDS Benchmark

The proposed Motion Difficulty Score (MDS) benchmark advances motion imitation evaluation and its broader applications by modeling motion-intrinsic difficulty. In this section, we first present the definition of motion difficulty grounded in rigid-body dynamics (Sec. 4.1); Then, we quantify it into the proposed MDS (Sec. 4.2); Finally, we present MD-AMASS, a difficulty-stratified augmentation of the widely used AMASS dataset (Sec. 4.3).

4.1. Motion Difficulty Definition

From Eq. 1, it can be observed that for any state q , a perturbation in q induces a corresponding change in the torque space. Therefore, we define motion difficulty based on the following key insight: *The success of imitation learning hinges on how strongly the required torques vary under small motion perturbations.* Specifically, when tiny pose deviations trigger large torque changes, reinforcement learning (and gradient-based optimization) encounters flat or plateau-like reward (and loss) landscapes: substantial torque updates produce nearly identical poses and thus yield nearly identical rewards. In such regions, the reward becomes weakly informative with respect to torque adjustments, providing little useful improvement signals. Intuitively, as illustrated in Fig. 2, for an easy motion such as a hand wave (Fig. 2 top left), a small positional change induces only a mild torque adjustment, and the policy receives clear improvement signals. For a difficult motion such as a single-leg stance (Fig. 2 bottom left), the reward landscape collapses into a Dirac-delta-like spike, where reward is concentrated within an extremely narrow region and flattens almost immediately elsewhere. In this regime, the policy explores torque updates in many directions on the plateau,

yet the resulting rewards are nearly identical. We therefore define the imitation difficulty of a motion S as the magnitude of torque variation induced within a bounded pose-error neighborhood:

Definition 4.1 (Motion Difficulty). Let $s = (q, \dot{q}, \ddot{q})$ denote the per-frame character state. For a motion sequence $S = (s_1, \dots, s_t)$ of length t , let $F : X \rightarrow Y$ maps states S in $X = \mathbb{R}^{N \times 3 \times t}$ to torques T in $Y = \mathbb{R}^{J \times t}$. Accordingly, we have $\mathcal{T} = \{T | T = F(\hat{S}), \hat{S} \in \mathcal{N}(S)\}$, where \mathcal{T} is the torque variation induced by $\mathcal{N}(S)$, which denotes the local neighborhood of perturbed states around S . The **Motion Difficulty** of S , i.e., the magnitude of torque variations, can then be characterized by the following three factors:

1. The overall **volume** $\text{vol}_Y(\mathcal{T})$, reflecting the total torque variation induced by pose perturbations;
2. The **variance** of \mathcal{T} across joint dimensions, capturing the geometric spread in per-joint torque variation;
3. The **temporal variability** of \mathcal{T} over the entire sequence, measuring how torque variations evolve across time.

4.2. Motion Difficulty Score

In this section, we formalize the computation of the proposed Motion Difficulty Score (MDS) based on the theoretical foundation established in Sec. 4.1. Specifically, we model the three factors in Definition 4.1 using three complementary diversity metrics and aggregate them to produce the final Motion Difficulty Score (MDS), reflecting the inherent imitation difficulty of the motion. Readers may refer to Fig. 2 for a more intuitive understanding of the diversity metrics.

4.2.1. Spectral Diversity

For a given motion sequence S , spectral diversity is used to model the volume $\text{vol}_Y(\mathcal{T})$, i.e., the Lebesgue measure in

torque space. By applying the coarea formula and normalizing by $\text{vol}_X(\mathcal{N}(S))$, we have :

$$\text{vol}_Y(\mathcal{T}) \propto [\text{vol}_X(\mathcal{N}(S))]^{1/3} \cdot \prod_{i=1}^t \sqrt{\det(G_i)}, \quad (2)$$

where $G_i = dF_i(s_i) dF_i(s_i)^T$. Thus, the volume $\text{vol}_Y(\mathcal{T})$ is determined by $\prod_{i=1}^t \sqrt{\det(G_i)}$.

Summing over all frames, the log-volume of the total torque variation is:

$$\log \text{vol}_Y(\mathcal{T}) \propto \sum_{i=1}^r \log \sigma_i. \quad (3)$$

where $r = \min(t, J \cdot D)$. This shows that the total torque variation grows with the sum of log-singular values across all joints and frames.

Thus, we define **Spectral Diversity** as:

$$d_1 = \sum_{i=1}^r (\log \sigma_i), \quad (4)$$

Spectral Diversity thus captures the effective dimensionality of the feasible torque space, higher values indicating higher torque variation and higher difficulty. Due to space constraints, we provide the detailed derivation for the log-volume of torque variation in the **supplementary materials**.

4.2.2. Variance Diversity

Eq. 18 shows that the volume of the torque space is directly related to G_i , hence to the Jacobian matrix $J = dF_i$. Therefore, we define **Variance Diversity** as the variation of the Jacobian across different joints:

$$d_2 = \sum_{j=1}^J \log(\text{Var}_j), \quad (5)$$

where:

$$\text{Var}_j = \mathbb{E}_{t,k}[\mathbf{J}_{t,j,k}^2] - (\mathbb{E}_{t,k}[\mathbf{J}_{t,j,k}])^2, \quad (6)$$

and t is the time index, k is the index over rotation directions. The variance Var_j quantifies the spread in torque variation for joint j , and d_2 aggregates this across all joints via a geometric mean. Because variance in the Jacobian entries corresponds to the magnitude of singular values, Variance Diversity captures the extent of joint-wise torque variation, where smaller variance signifies higher motion difficulty.

4.2.3. Segment Diversity

To capture temporal evolution of torque variations, we partition the motion sequence into K non-overlapping subsequences and compute **Segment Diversity** as the sum of

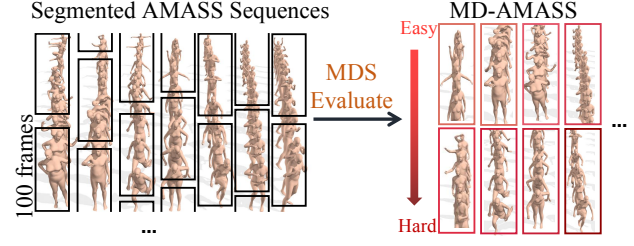


Figure 3. Our Difficulty-aware AMASS Dataset MD-AMASS.

spectral diversity per segment:

$$d_3 = \frac{1}{K} \sum_{k=1}^K d_1(J_k) \propto \frac{1}{K} \sum_{k=1}^K \log V_s = \log \left(\prod_{s=1}^S V_s \right)^{1/S}, \quad (7)$$

where J_k is the Jacobian sequence in segment k . From inequality of arithmetic and geometric mean, we have:

$$d_3 \propto \log \left(\prod_{s=1}^S V_s \right)^{1/S} \leq \frac{1}{S} \sum_{s=1}^S V_s. \quad (8)$$

The upper bound of the inequality is attained if and only if $d_1(J_1) = d_1(J_2) = \dots = d_1(J_K)$, at which point the segment diversity reaches its maximum value. This means that for a motion sequence S with fixed total torque volume, d_3 is maximized when all segments have equal volume, hence more difficult to imitate, consistent with the *Temporal Variability* factor. Conversely, d_3 decreases as the volume disparity between segments grows. Intuitively, a motion containing both relatively easy and difficult segments can facilitate learning because these segments are correlated: progress on the easier portions provides intermediate structure that guides the policy toward successfully handling the more challenging parts. For instance, in a kicking motion, the initial weight-shifting and leg-lifting phases are relatively easy, while the final fast extension and balance recovery are more difficult. As the policy masters the easier early phases, it gains stable trajectories and meaningful reward signals that guide it toward successfully learning the harder components. Empirically, we set $K = 4$ in our experiments to effectively capture temporal dynamics.

4.2.4. Final Formulation

The final Motion Difficulty Score (MDS) is computed as the weighted sum of the three diversity terms, the weight assignments are empirically derived:

$$\text{MDS} = \sum_{i=1}^3 w_i d_i, \quad (9)$$

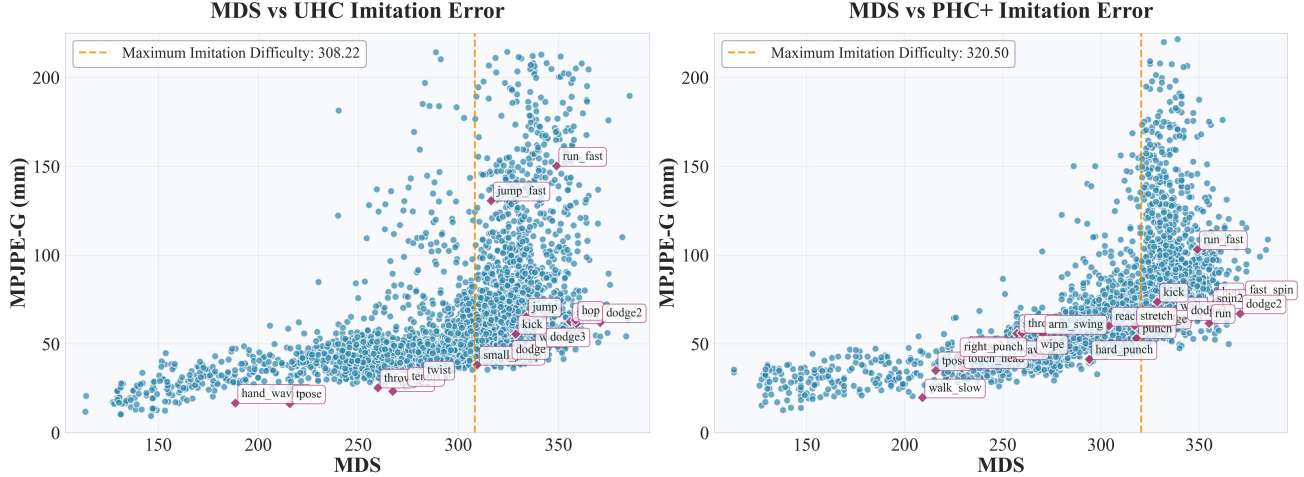


Figure 4. We plot scatters of MDS versus imitation error on different policies for over 3000 motion clips (left: UHC; right: PHC+), with samples drawn from the policies’ training set. As MDS increases from left to right (indicating higher difficulty), error rises from bottom to top, demonstrating that MDS effectively captures motion difficulty.

4.3. Motion Difficulty-aware Database

Building on the Motion Difficulty Score (MDS) introduced in Sec. 4.2, we present **MD-AMASS**, a motion difficulty-aware extension of the widely used AMASS dataset [], enabling difficulty-conditioned benchmarking for motion imitation and related tasks. Specifically, to ensure compatibility with imitation learning, we follow the sequence partitioning strategy illustrated in Fig. 3 and segment the AMASS dataset into fixed-length clips of 100 frames (approximately 3.3 seconds at 30 FPS). This design choice mitigates intra-sequence difficulty variation: longer sequences often contain diverse sub-actions with differing challenges, which would blur per-clip difficulty assessment. By using short, homogeneous clips, we achieve more precise and meaningful difficulty estimation. For each sequence, we extend it with the MDS computed using the method described in Sec. 4.2. Per-frame inertial matrices M and nonlinear dynamics terms h are computed using the Rigid Body Dynamics Library (RBDL) [13], with pose perturbations iteratively applied along the sequence.

In summary, MD-AMASS comprises over 30,000 short motion sequences, each annotated with a scalar difficulty coefficient, along with a modular MDS computation pipeline that can be directly applied to arbitrary motion data or alternative segmentation schemes. This enables seamless extension to other datasets or customized sequence lengths.

5. Validation of the MDS Benchmark

Our validation focuses on rigorously confirming the predictive power of our Motion Difficulty Score (MDS). First, we validate our MDS by assessing its consistency with the results of state-of-the-art imitation policies (Sec. 5.1). The re-

sults show a strong correlation between MDS and imitation error: motions with higher MDS yield larger tracking errors, while lower MDS indicates easier imitation and lower error. Then, we conduct an ablation study to understand the contribution of each component of MDS (Sec. 5.2). Results show that partial formulations fail to capture true difficulty patterns, while the complete MDS best aligns with observed imitation outcomes.

5.1. Consistency with Imitation Results

Our experiments are conducted on state-of-the-art imitation learning policies UHC and PHC+, using our MD-AMASS dataset as the evaluation benchmark.

Statistical Visualization. In Fig. 4, we visualize over 3,000 randomly sampled sequences, with the x -axis showing the MDS score (higher = more difficult) and the y -axis representing imitation error (global root-relative Mean Per-Joint Position Error (MPJPE-G) in mm, reflecting policy accuracy). To maintain visual clarity and focus on typical operating regimes, we exclude a small set of extreme outliers (fewer than 100 clips) where both MPJPE-G exceeds 250 mm *and* MDS exceeds 350, as these represent near-failure cases. A strong positive correlation is observed for both UHC (Fig. 4, left) and PHC+ (Fig. 4, right), confirming the effectiveness of MDS in quantifying motion difficulty. We provide analysis with more samples in the **supplementary materials**.

Quantitative Results. We further analyze this relationship in Table 1 (top) using three standard correlation metrics: 1) **Pearson’s r** , which measures *linear* correlation between predicted difficulty and imitation error ($r \in [-1, 1]$); values near 1 indicate strong positive linearity, while $r \approx 0$ sug-

Table 1. Correlation between Motion Difficulty Score (MDS) and Imitation Error (MPJPE-G) on UHC and PHC+. Motions are sorted by increasing MDS. Higher MDS consistently predicts higher tracking error across both models, validating our difficulty metric.

Correlation	UHC						PHC+					
	Pearson		Spearman		Kendall		Pearson		Spearman		Kendall	
	0.4823		0.6586		0.4747		0.6478		0.8203		0.6293	
Samples	Motion	MDS	MPJPE-G	Motion	MDS	MPJPE-G	Motion	MDS	MPJPE-G	Motion	MDS	MPJPE-G
		hand_waving	188.58	16.67	tpose	215.71	16.34	walk_slow	209.82	19.75	touch_head	229.73
	tpose2	267.20	23.29	throw	259.71	25.28	wave	225.34	41.23	right_punch	227.89	43.77
	tennis	273.48	26.20	twist	270.28	29.77	spin	257.09	55.98	wipe	266.71	44.28
	small_jump	309.36	38.21	dodge	325.62	41.42	throw	259.71	56.15	small_step	280.27	50.23
	walk	337.27	48.20	kick	328.67	55.56	reach_high	304.39	60.17	punch	318.90	53.17
	dodge2	342.72	48.45	jump	333.87	65.31	stretch	317.90	60.52	walk	337.27	65.85
	spin2	355.95	62.57	run	358.97	61.47	run	355.76	61.67	kick	328.67	73.65
	hop	358.54	63.40	spin2	355.95	62.56	run_fast	349.02	103.23	hop	358.54	73.85
	fast_jump	316.30	130.68	run_fast	349.02	150.21	spin2	355.95	70.10	fast_spin	372.48	75.00

gests no linear relationship; 2) **Spearman’s ρ** , a rank-based metric evaluating *monotonic* relationships ($[-1, 1]$); high ρ reflects consistent difficulty-error ordering; 3) **Kendall’s τ** , another rank correlation that counts concordant vs. discordant pairs ($[-1, 1]$); it is robust to outliers and emphasizes relative ordering agreement. The consistently high correlations across both models strongly validate MDS as a reliable model of motion difficulty. To further illustrate MDS’s explanatory power, we select representative samples and include their MDS and MPJPE-G values in Table 1 (bottom).

Qualitative Results. In Fig. 5, we show representative motion samples with large difficulty gaps, ordered from easy (left) to hard (right). For example, a small forward step (Fig. 5 left 1) is rated easy and reproduced nearly perfectly. In contrast, high-MDS (>350) motions show clear degradation: in dodging (Fig. 5 right 4) and single-leg hopping (Fig. 5 right 2), the robot over-bends limbs to maintain balance; in a fast spinning dance (Fig. 5 right 1), leg flexion falls short of the reference. From the MDS definition, we interpret this as extreme torque variation: when small pose changes demand drastically different torques, the policy cannot produce the precise, hard-to-learn torque profile. Instead, it settles for a simpler torque that stabilizes the robot at a distant pose, *trading precision for stability*.

5.2. Ablation Study

We validate the necessity of our diversity aggregation design and the three diversity models using the aforementioned standard correlation metrics. In Table 2, we conduct ablation studies on the three diversity proxies Spectral Diversity (*w/o SP*), Variance Diversity (*w/o VA*), Segment Diversity (*w/o SE*), demonstrating the correlation between these configurations and imitation errors for both PHC+ and UHC. The results clearly shows that any partial combination yields lower correlation with policy performance than the full MDS, rendering them insufficient as standalone difficulty predictors. Notably, Spearman’s ρ exceeds 0.5

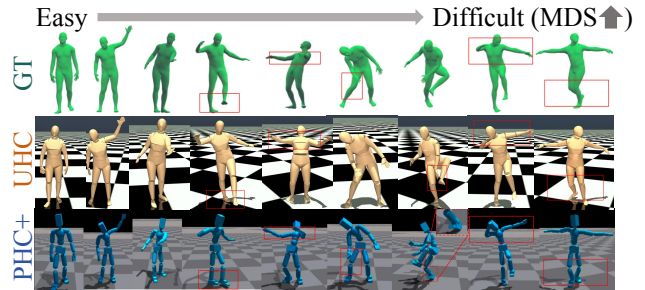


Figure 5. Imitation fidelity visibly degrades as MDS increases, validating MDS as an accurate model of motion difficulty.

Table 2. Difficulty-Error Correlation Coefficients Study on Diversity Aggregation Design

Score	Pearson	Spearman	Kendall
UHC			
<i>w/o VA</i>	0.4455	0.6218	0.4443
<i>w/o SE</i>	0.4475	0.6231	0.4455
<i>w/o SP</i>	0.4126	0.5847	0.4149
MDS(ours)	0.4823	0.6586	0.4747
PHC+			
<i>w/o VA</i>	0.6006	0.7963	0.6005
<i>w/o SE</i>	0.6026	0.7966	0.6014
<i>w/o SP</i>	0.5760	0.7803	0.5867
MDS(ours)	0.6478	0.8203	0.6293

across most configurations, indicating a robust *monotonic* relationship between the diversity models (and MDS) and imitation error, thereby validating the core principle of our diversity aggregation design.

6. Benchmarking Motion Imitation with MDS

After validating the effectiveness of our MDS (Sec. 5), we use it to benchmark state-of-the-art human motion imitation

policies from a *difficulty-aware* perspective, revealing insights unattainable without MDS. Specifically, we introduce two MDS-based metrics: **Maximum Imitable Difficulty (MID)** and **Difficulty-Stratified Joint Error (DSJE)**.

6.1. Maximum Imitable Difficulty (MID)

Table 3. Difficulty-Stratified Joint Error (DSJE) at fixed MDS thresholds (mm).

Policy	DSJE-200	DSJE-300	DSJE-350
UHC	27.79	45.75	62.94
PHC+	30.38	39.01	59.50

Revisiting Fig. 4, we observe that while both UHC and PHC+ exhibit a strong overall positive correlation with MDS, a growing number of outliers emerge as difficulty increases. These are particularly evident on the right side of the scatter plots, where imitation error surges dramatically for high-MDS samples. The pattern is also reflected in Table 1 (e.g., *run_fast*). Such outliers signify a *breakdown in policy capability* on challenging motions, marking the onset of performance collapse.

To quantify this transition, we exhaustively evaluate all possible MDS split points (e.g., 100, 101, ..., up to the maximum) and, for each, compute the mean MPJPE-G of the left (low-difficulty) and right (high-difficulty) partitions. The split that *maximizes inter-group error disparity* defines the critical difficulty level at which large errors begin to dominate. We term this threshold the **Maximum Imitable Difficulty (MID)**, a direct measure of a policy’s robustness boundary. We formally define it as:

$$\text{MID} = \arg \max_{c \in \mathcal{C}} [\mu_{\text{high}}(c) - \mu_{\text{low}}(c)], \quad (10)$$

where:

- \mathcal{C} is the set of all candidate MDS thresholds;
- $\mathcal{D}_{\text{low}} = \{S \in \mathcal{S} | \text{MDS}(S) \leq c\}$ and $\mathcal{D}_{\text{high}} = \{S \in \mathcal{S} | \text{MDS}(S) > c\}$ are the low- and high-difficulty partitions, \mathcal{S} is set of all motion clips and $\text{MDS}(S)$ is MDS of S ;
- $\mu_{\text{low}}(c) = \frac{1}{|\mathcal{D}_{\text{low}}|} \sum_{S \in \mathcal{D}_{\text{low}}} \text{MPJPE-G}(S)$ is the mean imitation error for motions with $\text{MDS} \leq c$, $\text{MPJPE-G}(S)$ is MPJPE-G of S ;
- $\mu_{\text{high}}(c) = \frac{1}{|\mathcal{D}_{\text{high}}|} \sum_{S \in \mathcal{D}_{\text{high}}} \text{MPJPE-G}(S)$ is the mean imitation error for motions with $\text{MDS} > c$.

The MID thus identifies the precise MDS value where the *marginal increase in imitation error* is maximized, marking the boundary beyond which the policy’s performance degrades substantially. In Fig. 4, we mark the computed MID with red dashed lines: UHC achieves MID =

308.22, while PHC+ reaches MID = 320.50. This quantitatively confirms PHC+’s superior imitation capacity, with UHC exhibiting earlier onset of outliers, which is a distinction clearly visible in the plots.

6.2. Difficulty-Stratified Joint Error (DSJE)

Existing evaluation protocols typically report average policy error across the entire dataset. While this provides a useful summary of overall performance, we argue that it obscures critical insights: a lower mean error does not guarantee superiority on *every* motion, nor does it reveal where a policy truly excels or falters. To address this limitation, we introduce a difficulty-stratified evaluation using our proposed benchmark. Specifically, we define the Difficulty-Stratified Joint Error (DSJE, in mm) at increasing difficulty thresholds: 1) DSJE-200: error on easy motions (MDS < 200), 2) DSJE-300: error on moderate motions (MDS < 300), 3) DSJE-350: error on all motions up to high difficulty (MDS < 350).

The unified formulation for DSJE at threshold c is:

$$\text{DSJE-}c = \frac{1}{|\mathcal{M}_c|} \sum_{S \in \mathcal{M}_c} \text{MPJPE-G}(S), \quad (11)$$

where $\mathcal{M}_c = \{S \in \mathcal{S} | \text{MDS}(S) < c\}$, $|\mathcal{M}_c|$ denotes the number of motions in the difficulty-stratified subset.

These metrics are reported in Table 3 for both UHC and PHC+. While conventional aggregate evaluation confirms PHC+’s overall superiority over UHC, our DSJE analysis reveals a surprising counter-pattern: PHC+ underperforms UHC on the easiest motions (DSJE-200), despite outperforming on moderate and cumulative sets. This novel finding emerged only through our difficulty-aware lens, and offers deeper diagnostic value. It enables precise characterization of policy behavior, training dynamics, and task-specific applicability: *which model is best suited for which difficulty regime?* Such insights pave the way for targeted improvements, curriculum design, and principled deployment in real-world humanoid control.

7. Conclusion and Limitations

Conclusion. In this work, we introduced the Motion Difficulty Score (MDS), a principled measure of imitation difficulty of a motion grounded in rigid-body dynamics and defined through torque variation under small pose perturbations. By modeling three key properties of the induced torque space: volume, variance, and temporal variability, MDS provides a motion-centric perspective that complements traditional similarity-based metrics. Using MDS, we also constructed MD-AMASS, a difficulty-aware repartitioning of the AMASS dataset. Our experiments show that MDS reliably explains performance trends of state-of-the-art imitation policies, and the MDS-derived MID and DSJE

metrics further highlight its diagnostic value.

Limitation. The computation of the inertial matrices M and nonlinear dynamics terms h in Eq. 1 relies on the C++ library RBDL [13], which serves as a computational bottleneck of our MDS (processing a 100-frame motion sequence takes roughly 1–2 minutes on an Intel(R) Core(TM) i9-14900KF CPU). Since RBDL is not optimized for GPU parallelism, our MDS inherits this constraint and computes these terms on the CPU. We expect that integrating faster or GPU-accelerated libraries could further improve the efficiency of our MDS.

8. Acknowledgments

This work is supported by National Natural Science Foundation of China (62472364, 62072383), the Public Technology Service Platform Project of Xiamen City (No.3502Z20231043), Xiaomi Young Talents Program / Xiaomi Foundation and the Fundamental Research Funds for the Central Universities (20720240058), “Young Eagle Plan” Top Talents of Fujian Province. Anjun Chen is the corresponding author.

References

- [1] Firas Al-Hafez, Guoping Zhao, Jan Peters, and Davide Tateo. Locomujoco: A comprehensive imitation learning benchmark for locomotion. *arXiv preprint arXiv:2311.02496*, 2023. 3
- [2] Georgios Albanis, Nikolaos Zioulis, Spyridon Thermos, Anargyros Chatzitofis, and Kostas Kolomvatsos. Noise-in, bias-out: Balanced and real-time mocap solving, 2023. 13
- [3] Andreas Aristidou, Ariel Shamir, and Yiorgos Chrysanthou. Digital dance ethnography: Organizing large dance collections. *J. Comput. Cult. Herit.*, 12(4), Nov. 2019. 3
- [4] Yoshua Bengio, Jérôme Louradour, Ronan Collobert, and Jason Weston. Curriculum learning. In *Proceedings of the 26th Annual International Conference on Machine Learning, ICML ’09*, page 41–48, New York, NY, USA, 2009. Association for Computing Machinery. 13
- [5] Kevin Bergamin, Simon Clavet, Daniel Holden, and James Richard Forbes. Drecon: data-driven responsive control of physics-based characters. *ACM Transactions On Graphics (TOG)*, 38(6):1–11, 2019. 2
- [6] Zhongang Cai, Daxuan Ren, Ailing Zeng, Zhengyu Lin, Tao Yu, Wenjia Wang, Xiangyu Fan, Yang Gao, Yifan Yu, Liang Pan, et al. Humman: Multi-modal 4d human dataset for versatile sensing and modeling. In *European Conference on Computer Vision*, pages 557–577. Springer, 2022. 3
- [7] Carnegie Mellon University. CMU MoCap Dataset. 2, 3
- [8] Yu-Wei Chao, Jimei Yang, Weifeng Chen, and Jia Deng. Learning to sit: Synthesizing human-chair interactions via hierarchical control. In *Proceedings of the AAAI Conference on Artificial Intelligence*, volume 35, pages 5887–5895, 2021. 3
- [9] Nuttapon Chentanez, Matthias Müller, Miles Macklin, Viktor Makoviychuk, and Stefan Jeschke. Physics-based motion capture imitation with deep reinforcement learning. In *Proceedings of the 11th ACM SIGGRAPH Conference on Motion, Interaction and Games*, pages 1–10, 2018. 2, 3
- [10] Jihoon Chung, Cheng-hsin Wu, Hsuan-ru Yang, Yu-Wing Tai, and Chi-Keung Tang. Haa500: Human-centric atomic action dataset with curated videos. In *Proceedings of the IEEE/CVF international conference on computer vision*, pages 13465–13474, 2021. 3
- [11] Zhiyang Dou, Xuelin Chen, Qingnan Fan, Taku Komura, and Wenping Wang. C-case: Learning conditional adversarial skill embeddings for physics-based characters. *arXiv preprint arXiv:2309.11351*, 2023. 2
- [12] Roy Featherstone. *Rigid body dynamics algorithms*. Springer, 2008. 2, 3
- [13] Martin L. Felis. RbdL: an efficient rigid-body dynamics library using recursive algorithms. *Auton. Robots*, 41(2):495–511, Feb. 2017. 6, 9
- [14] Levi Fussell, Kevin Bergamin, and Daniel Holden. Super-track: Motion tracking for physically simulated characters using supervised learning. *ACM Transactions on Graphics (TOG)*, 40(6):1–13, 2021. 2
- [15] Kehong Gong, Bingbing Li, Jianfeng Zhang, Tao Wang, Jing Huang, Michael Bi Mi, Jiashi Feng, and Xinchao Wang. Posetriplet: Co-evolving 3d human pose estimation, imitation, and hallucination under self-supervision. In *Proceedings of the IEEE/CVF conference on computer vision and pattern recognition*, pages 11017–11027, 2022.
- [16] Leonard Hasenclever, Fabio Pardo, Raia Hadsell, Nicolas Heess, and Josh Merel. Comic: Complementary task learning & mimicry for reusable skills. In *International Conference on Machine Learning*, pages 4105–4115. PMLR, 2020. 2
- [17] Fabian Helm, Nikolaus F. Troje, and Jörn Munzert. Motion database of disguised and non-disguised team handball penalty throws by novice and expert performers. *Data in Brief*, 15:981–986, 2017. 3
- [18] Yinghao Huang, Manuel Kaufmann, Emre Aksan, Michael J. Black, Otmar Hilliges, and Gerard Pons-Moll. Deep inertial poser learning to reconstruct human pose from sparse inertial measurements in real time. *ACM Transactions on Graphics, (Proc. SIGGRAPH Asia)*, 37(6):185:1–185:15, Nov. 2018. 15
- [19] Catalin Ionescu, Dragos Papava, Vlad Olaru, and Cristian Sminchisescu. Human3.6m: Large scale datasets and predictive methods for 3d human sensing in natural environments. *IEEE Transactions on Pattern Analysis and Machine Intelligence*, 36:1325–1339, 2014. 3
- [20] Kyungmin Lee, Sibeon Kim, Minhoo Park, Hyunseung Kim, Dongyoon Hwang, Hojoon Lee, and Jaegul Choo. Phuma: Physically-grounded humanoid locomotion dataset. *arXiv preprint arXiv:2510.26236*, 2025. 3
- [21] Ronghui Li, Junfan Zhao, Yachao Zhang, Mingyang Su, Zeping Ren, Han Zhang, Yansong Tang, and Xiu Li. Finedance: A fine-grained choreography dataset for 3d full body dance generation. In *Proceedings of the IEEE/CVF International Conference on Computer Vision (ICCV)*, pages 10234–10243, October 2023. 3
- [22] Jing Lin, Ailing Zeng, Shunlin Lu, Yuanhao Cai, Ruimao Zhang, Haoqian Wang, and Lei Zhang. Motion-x: A large-scale 3d expressive whole-body human motion

- dataset. *Advances in Neural Information Processing Systems*, 36:25268–25280, 2023. 3
- [23] Matthew Loper, Naureen Mahmood, Javier Romero, Gerard Pons-Moll, and Michael J Black. Smpl: A skinned multi-person linear model. In *Seminal Graphics Papers: Pushing the Boundaries, Volume 2*, pages 851–866. 2023. 3
- [24] Zhengyi Luo, Jinkun Cao, Kris Kitani, Weipeng Xu, et al. Perpetual humanoid control for real-time simulated avatars. In *Proceedings of the IEEE/CVF International Conference on Computer Vision*, pages 10895–10904, 2023. 1, 2, 3, 14
- [25] Zhengyi Luo, Jinkun Cao, Josh Merel, Alexander Winkler, Jing Huang, Kris Kitani, and Weipeng Xu. Universal humanoid motion representations for physics-based control. *arXiv preprint arXiv:2310.04582*, 2023. 1
- [26] Zhengyi Luo, Ryo Hachiuma, Ye Yuan, and Kris Kitani. Dynamics-regulated kinematic policy for egocentric pose estimation. *Advances in Neural Information Processing Systems*, 34:25019–25032, 2021. 1, 2, 14
- [27] Naureen Mahmood, Nima Ghorbani, Nikolaus F Troje, Gerard Pons-Moll, and Michael J Black. Amass: Archive of motion capture as surface shapes. In *Proceedings of the IEEE/CVF international conference on computer vision*, pages 5442–5451, 2019. 2, 3
- [28] Jiageng Mao, Siheng Zhao, Siqi Song, Chuye Hong, Tianheng Shi, Junjie Ye, Mingtong Zhang, Haoran Geng, Jitendra Malik, Vitor Guizilini, et al. Universal humanoid robot pose learning from internet human videos. In *2025 IEEE-RAS 24th International Conference on Humanoid Robots (Humanoids)*, pages 1–8. IEEE, 2025. 3
- [29] Josh Merel, Saran Tunyasuvunakool, Arun Ahuja, Yuval Tassa, Leonard Hasenclever, Vu Pham, Tom Erez, Greg Wayne, and Nicolas Heess. Catch & carry: reusable neural controllers for vision-guided whole-body tasks. *ACM Transactions on Graphics (TOG)*, 39(4):39–1, 2020. 2, 3
- [30] Yuxuan Mu, Hung Yu Ling, Yi Shi, Ismael Baira Ojeda, Pengcheng Xi, Chang Shu, Fabio Zinno, and Xue Bin Peng. Stablemotion: Training motion cleanup models with unpaired corrupted data, 2025. 13
- [31] Soohwan Park, Hoseok Ryu, Seyoung Lee, Sunmin Lee, and Jehee Lee. Learning predict-and-simulate policies from unorganized human motion data. *ACM Transactions on Graphics (TOG)*, 38(6):1–11, 2019. 3
- [32] Georgios Pavlakos, Vasileios Choutas, Nima Ghorbani, Timo Bolkart, Ahmed AA Osman, Dimitrios Tzionas, and Michael J Black. Expressive body capture: 3d hands, face, and body from a single image. In *Proceedings of the IEEE/CVF conference on computer vision and pattern recognition*, pages 10975–10985, 2019. 3
- [33] Xue Bin Peng, Pieter Abbeel, Sergey Levine, and Michiel Van de Panne. Deepmimic: Example-guided deep reinforcement learning of physics-based character skills. *ACM Transactions On Graphics (TOG)*, 37(4):1–14, 2018. 2, 3
- [34] Xue Bin Peng, Glen Berseth, KangKang Yin, and Michiel Van De Panne. Deeploco: Dynamic locomotion skills using hierarchical deep reinforcement learning. *Acm transactions on graphics (TOG)*, 36(4):1–13, 2017. 2, 3
- [35] Xue Bin Peng, Michael Chang, Grace Zhang, Pieter Abbeel, and Sergey Levine. Mcp: Learning composable hierarchical control with multiplicative compositional policies. *Advances in neural information processing systems*, 32, 2019.
- [36] Xue Bin Peng, Yunrong Guo, Lina Halper, Sergey Levine, and Sanja Fidler. Ase: Large-scale reusable adversarial skill embeddings for physically simulated characters. *ACM Transactions On Graphics (TOG)*, 41(4):1–17, 2022. 2
- [37] Xue Bin Peng, Angjoo Kanazawa, Jitendra Malik, Pieter Abbeel, and Sergey Levine. Sfv: Reinforcement learning of physical skills from videos. *ACM Transactions On Graphics (TOG)*, 37(6):1–14, 2018. 3
- [38] Xue Bin Peng, Ze Ma, Pieter Abbeel, Sergey Levine, and Angjoo Kanazawa. Amp: Adversarial motion priors for stylized physics-based character control. *ACM Transactions on Graphics (TOG)*, 40(4):1–20, 2021. 2, 3
- [39] Yunzhe Shao, Xinyu Yi, Lu Yin, Shihui Guo, Junhai Yong, and Feng Xu. Magshield: Towards better robustness in sparse inertial motion capture under magnetic disturbances. In *Proceedings of the IEEE/CVF International Conference on Computer Vision (ICCV)*, pages 29021–29030, October 2025. 15
- [40] Soshi Shimada, Vladislav Golyanik, Weipeng Xu, and Christian Theobalt. Physcap: Physically plausible monocular 3d motion capture in real time. *ACM Transactions on Graphics*, 39(6), dec 2020. 3
- [41] Petru Soviany, Radu Tudor Ionescu, Paolo Rota, and Nicu Sebe. Curriculum learning: A survey. *Int. J. Comput. Vision*, 130(6):1526–1565, June 2022. 14
- [42] Shuhei Tsuchida, Satoru Fukayama, Masahiro Hamasaki, and Masataka Goto. Aist dance video database: Multi-genre, multi-dancer, and multi-camera database for dance information processing. In *ISMIR*, volume 1, page 6, 2019. 3
- [43] Unitree Robotics. Unitree G1 humanoid robot. <https://www.unitree.com/cn/g1>, 2024. Accessed: 2025-11-17. 14
- [44] Nolan Wagener, Andrey Kolobov, Felipe Vieira Frujeri, Ricky Loynd, Ching-An Cheng, and Matthew Hausknecht. Mocapact: A multi-task dataset for simulated humanoid control. *Advances in Neural Information Processing Systems*, 35:35418–35431, 2022. 2
- [45] Tingwu Wang, Yunrong Guo, Maria Shugrina, and Sanja Fidler. Unicon: Universal neural controller for physics-based character motion. *arXiv preprint arXiv:2011.15119*, 2020. 2
- [46] Alexander Winkler, Jungdam Won, and Yuting Ye. Questsim: Human motion tracking from sparse sensors with simulated avatars. In *SIGGRAPH Asia 2022 Conference Papers*, pages 1–8, 2022. 2
- [47] Jungdam Won, Deepak Gopinath, and Jessica Hodgins. A scalable approach to control diverse behaviors for physically simulated characters. *ACM Transactions on Graphics (TOG)*, 39(4):33–1, 2020. 2, 3
- [48] Heyuan Yao, Zhenhua Song, Baoquan Chen, and Libin Liu. Controlvae: Model-based learning of generative controllers for physics-based characters. *ACM Trans. Graph.*, 41(6), 2022. 2
- [49] Heyuan Yao, Zhenhua Song, Yuyang Zhou, Tenglong Ao, Baoquan Chen, and Libin Liu. Moconvq: Unified physics-based motion control via scalable discrete representations. *ACM Trans. Graph.*, 43(4), July 2024. 2
- [50] Lu Yin, Ziyang Shi, Yinghao Wu, Xinyu Yi, Feng Xu, and Shihui Guo. Shape-aware inertial poser: Motion tracking

for humans with diverse shapes using sparse inertial sensors, 2025. 14, 15

- [51] Ye Yuan and Kris Kitani. Ego-pose estimation and forecasting as real-time pd control. In *Proceedings of the IEEE/CVF International Conference on Computer Vision*, pages 10082–10092, 2019. 2
- [52] Ye Yuan and Kris Kitani. Residual force control for agile human behavior imitation and extended motion synthesis. *Advances in Neural Information Processing Systems*, 33:21763–21774, 2020. 2, 3
- [53] Yanjie Ze, Zixuan Chen, João Pedro Araújo, Zi ang Cao, Xue Bin Peng, Jiajun Wu, and C. Karen Liu. Twist: Teleoperated whole-body imitation system. *arXiv preprint arXiv:2505.02833*, 2025. 14
- [54] Siwei Zhang, Qianli Ma, Yan Zhang, Zhiyin Qian, Taemin Kwon, Marc Pollefeys, Federica Bogo, and Siyu Tang. Ego-body: Human body shape and motion of interacting people from head-mounted devices. In *European conference on computer vision*, pages 180–200. Springer, 2022. 3
- [55] Youliang Zhang, Ronghui Li, Yachao Zhang, Liang Pan, Jingbo Wang, Yebin Liu, and Xiu Li. A plug-and-play physical motion restoration approach for in-the-wild high-difficulty motions. In *Proceedings of the IEEE/CVF International Conference on Computer Vision (ICCV)*, pages 13281–13292, October 2025. 3
- [56] Yuhong Zhang, Jing Lin, Ailing Zeng, Guanlin Wu, Shunlin Lu, Yurong Fu, Yuanhao Cai, Ruimao Zhang, Haoqian Wang, and Lei Zhang. Motion-x++: A large-scale multimodal 3d whole-body human motion dataset. *arXiv preprint arXiv:2501.05098*, 2025. 3
- [57] Yu Zheng and Katsu Yamane. Human motion tracking control with strict contact force constraints for floating-base humanoid robots. In *2013 13th IEEE-RAS International Conference on Humanoid Robots (Humanoids)*, pages 34–41, 2013. 3
- [58] Chengxu Zuo, Jiawei Huang, Xiao Jiang, Yuan Yao, Xiangren Shi, Rui Cao, Xinyu Yi, Feng Xu, Shihui Guo, and Yipeng Qin. Transformer imu calibrator: Dynamic on-body imu calibration for inertial motion capture. *ACM Trans. Graph.*, 44(4), July 2025. 13, 15

A. Spectral Diversity Details

Following the definitions from the main paper, we complete the detailed proofs and definitions for the relevant propositions regarding spectral diversity, including:

- definition of the torque space volume $\text{vol}_Y(\mathcal{T})$
- the relationship between $\text{vol}_Y(\mathcal{T})$ and the Gram determinant $\det(G_i)$ (Equation 2);
- computation of the $\det(G_i)$.

A.1. Torque Space Volume Definition

We first revisit the problem setup. Let $S = (s_1, s_2, \dots, s_t)$ be a motion sequence of t frames, where the state at frame i is $s_i = (q_i, \dot{q}_i, \ddot{q}_i)$, with q_i denoting position and rotation, \dot{q}_i and \ddot{q}_i are the generalized velocity and acceleration, respectively. Given $\dim q = N$, $F : X \rightarrow Y$ maps states S

in $X = \mathbb{R}^{N \times 3 \times t}$ to torques T in $Y = \mathbb{R}^{J \times t}$, where J is the number of joints.

Here, $F : X \rightarrow Y$ is defined by the rigid-body motion equation described in Section 3 of the main paper:

$$\tau = F(S) = M(q)\ddot{q} + h(q, \dot{q}) - f_{ext}, \quad (12)$$

and for each frame i ,

$$\tau_i = F_i(s_i) = M(q_i)\ddot{q}_i + h(q_i, \dot{q}_i) - f_{ext}. \quad (13)$$

When S is perturbed, we define the neighborhood $\mathcal{N}(S)$ as the Cartesian product of ϵ -balls centered at each reference state $s_i \in S$:

$$\mathcal{N}(S) = \prod_{i=1}^t B_\epsilon(s_i). \quad (14)$$

The image set $\mathcal{T} = F(\mathcal{N}(S))$ is then

$$\mathcal{T} = \prod_{i=1}^t F_i(B_\epsilon(s_i)). \quad (15)$$

Volume computation involves the volumes of the state space X and torque space Y . Since q includes rotations, S is a manifold, so the volume of a local ball scales as

$$\text{vol}_S(B_\epsilon(s_i)) \propto \epsilon^{3N}, \quad (16)$$

with the constant determined by the induced metric at s_i . Consequently,

$$\text{vol}_X(\mathcal{N}(S)) \propto \epsilon^{3Nt}. \quad (17)$$

The volume $\text{vol}_Y(\mathcal{T})$ is the Lebesgue measure in Y .

A.2. Volume Transformation and the Gram Determinant

In this section, we elaborate on Equation (2) introduced in Section 4.2.1 of the main paper and prove the relationship between the torque space volume and the Gram determinant G_i .

Proposition A.1. *For a given motion sequence S , the volume of the torque variation \mathcal{T} induced by $\mathcal{N}(S)$ satisfies:*

$$\text{vol}_Y(\mathcal{T}) \propto [\text{vol}_X(\mathcal{N}(S))]^{1/3} \cdot \prod_{i=1}^t \sqrt{\det(G_i)}, \quad (18)$$

where $G_i = dF_i(s_i) dF_i(s_i)^T$. Thus, the volume $\text{vol}_Y(\mathcal{T})$ is determined by $\prod_{i=1}^t \sqrt{\det(G_i)}$.

Proof. For the per-frame mapping $F_i : S \rightarrow \mathbb{R}^N$ with $\dim S = 3N > N$, if F_i is a submersion at s_i (i.e., its differential $dF_i(s_i)$ is surjective), then for sufficiently small

ϵ , the volume of the image set in \mathbb{R}^N is approximated by the coarea formula as

$$\text{vol}_{\mathbb{R}^N}(F_i(B_\epsilon(s_i))) \approx \text{vol}_S(B_\epsilon(s_i)) \cdot \sqrt{\det(dF_i(s_i) dF_i(s_i)^T)}, \quad (19)$$

where $dF_i(s_i) \in \mathbb{R}^{N \times 3N}$ is the Jacobian of F_i at s_i . The Gram matrix $dF_i(s_i) dF_i(s_i)^T \in \mathbb{R}^{N \times N}$ encodes local volume distortion, and its determinant’s square root governs the scaling factor. Since \mathcal{T} is a product space, the total volume is the product of per-frame contributions:

$$\begin{aligned} \text{vol}_Y(\mathcal{T}) &\approx \prod_{i=1}^t \text{vol}_{\mathbb{R}^N}(F_i(B_\epsilon(s_i))) \\ &\approx \prod_{i=1}^t [\text{vol}_S(B_\epsilon(s_i)) \cdot \sqrt{\det(G_i)}]. \end{aligned} \quad (20)$$

Substituting the manifold volume scaling $\text{vol}_S(B_\epsilon(s_i)) \propto \epsilon^{3N}$, we obtain

$$\text{vol}_Y(\mathcal{T}) \propto \epsilon^{Nt} \cdot \prod_{i=1}^t \sqrt{\det(G_i)}. \quad (21)$$

Given that the state-space neighborhood volume scales as $\text{vol}_X(\mathcal{N}(S)) \propto \epsilon^{3Nt}$, normalizing yields the ϵ -independent relation same as Eq. 18:

$$\text{vol}_Y(\mathcal{T}) \propto [\text{vol}_X(\mathcal{N}(S))]^{1/3} \cdot \prod_{i=1}^t \sqrt{\det(G_i)}. \quad (22)$$

Since $[\text{vol}_X(\mathcal{N}(S))]^{1/3}$ remains constant for motion sequences of the same length, the volume $\text{vol}_Y(\mathcal{T})$ is determined by $\prod_{i=1}^t \sqrt{\det(G_i)}$. \square

A.3. Computation of the Gram Determinant

Proposition A.2. *Derived from Eq. 22, the log-volume of the torque variation is:*

$$\log \text{vol}_Y(\mathcal{T}) \propto \sum_{i=1}^r \log \sigma_i. \quad (23)$$

where $r = \min(t, J \cdot D)$, and $D = \dim S = 3N$.

Proof. For each frame, the Jacobian matrix $dF_i \in \mathbb{R}^{N \times D}$ yields a Gram matrix that is an $N \times N$ symmetric positive definite matrix (since the inertial matrix $M(q)$ ensures that dF_i has full row rank). Let the Singular Value Decomposition (SVD) of dF_i be $dF_i = U_i \Sigma_i V_i^T$, where $\Sigma_i = \text{diag}(\sigma_{i,1}, \sigma_{i,2}, \dots, \sigma_{i,N})$, and $\sigma_{i,j} \geq 0$ are the singular values. Accordingly, we have:

$$G_i = U_i \Sigma_i \Sigma_i^T U_i^T = U_i \cdot \text{diag}(\sigma_{i,1}^2, \sigma_{i,2}^2, \dots, \sigma_{i,N}^2) \cdot U_i^T, \quad (24)$$

Therefore, we have:

$$\det(G_i) = \prod_{j=1}^N \sigma_{i,j}^2, \quad \sqrt{\det(G_i)} = \prod_{j=1}^N \sigma_{i,j}. \quad (25)$$

Taking the logarithm:

$$\log \sqrt{\det(G_i)} = \sum_{j=1}^N \log \sigma_{i,j}. \quad (26)$$

Summing over all frames, the log-volume of the total torque variation is:

$$\log \text{vol}_Y(\mathcal{T}) \propto \sum_{i=1}^r \log \sigma_i. \quad (27)$$

where $r = \min(t, J \cdot D)$. \square

Table 4. Quantitative comparison results between MDS-guided curriculum learning model (Ours) and baseline model (w/o CL).

Method	MPJPE-G (mm) ↓	MPJPE-L (mm) ↓	Acc-Dist (mm/frame ²) ↓	Vel-Dist (mm/frame) ↓
Overall Performance				
w/o CL	48.08	32.22	3.36	5.32
Ours	45.22	30.98	3.19	5.21
MDS < 200				
w/o CL	36.30	25.67	1.13	1.94
Ours	31.08	23.61	1.09	1.84
200 < MDS < 300				
w/o CL	49.94	35.04	3.04	4.96
Ours	49.52	35.43	2.93	4.83
MDS > 300				
w/o CL	60.79	37.44	6.32	9.65
Ours	59.18	35.90	5.87	9.52

B. Extensive Validation

To complement the validation in the main paper, we conduct an extensive evaluation on over 10,000 samples from the MD-AMASS dataset, enabling a more thorough examination of the effectiveness of MDS. Consistent with the validation results in the main paper, motions with higher MDS exhibit weaker policy performance, as shown in Fig. 6.

C. Applications

MDS has proven to be a powerful tool for in-depth evaluation of imitation learning policies, owing to its difficulty-aware nature. Nevertheless, beyond assessing model performance across motions of varying difficulty and deriving insightful metrics (e.g., MID and DSJE), MDS holds significant potential for broader applications, including:



Figure 6. More comprehensive scatter plots of MDS vs imitation error (top: UHC; bottom: PHC+), with over 10,000 motion samples drawn from the MD-AMASS dataset, providing stronger statistical evidence of the robust correlation between our proposed MDS and humanoid control error across different policy architectures.

1. *Difficulty-guided curriculum learning*: Simpler motions (those with lower MDS scores) are easier to learn and can be used in early training stages, with progressively higher-difficulty actions introduced later to improve learning efficiency and robustness.
2. *Generalization to other humanoid robots*.
3. *Detection of flawed motions in mocap datasets*: Many motion capture (mocap) systems produce noisy or physically implausible data, especially when sourced from video or IMU-based systems [2, 30, 58]. These flawed motions can be detected using MDS, as unusually high

MDS values may indicate corrupted or unrealistic motions (e.g., unnatural body contortions that violate physical constraints).

Preliminary results of these applications are shown below.

C.1. Difficulty-Guided Curriculum Learning

Curriculum learning [4] is a training paradigm that begins with simpler examples and progressively introduces more challenging ones, mimicking the natural progression of human learning. This structured, difficulty-ordered presentation of data has been shown to significantly accelerate

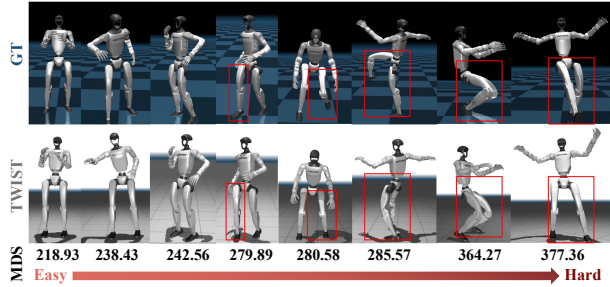


Figure 7. Qualitative results of the Unitree G1-based TWIST [53] controller on motions of increasing difficulty (easy \rightarrow hard, left \rightarrow right) as assessed by MDS. Red boxes highlight joints of noticeable imitation error.

convergence and enhance generalization in a wide range of tasks [41]. However, existing imitation-learning-based humanoid control approaches almost exclusively rely on random sampling of training motions, with virtually no attempts at curriculum learning. We argue that this gap stems from the absence of an explicit, quantitative definition of motion difficulty in prior work.

In this section, we present a simple yet revealing curriculum learning experiment. This experiment demonstrates that explicitly training the agent with motions ordered from easy to hard according to MDS leads to superior performance. Specifically, we sample 1000 motion sequences for each of three difficulty ranges from the MD-AMASS dataset: $MDS \leq 200$ (easy), $200 \leq MDS < 300$ (medium), and $MDS \geq 300$ (hard). We compare two training protocols using the PHC framework with a single primitive policy:

- **Baseline (Tab. 4 w/o CL):** All 3,000 sequences are mixed and trained jointly for 9,000 episodes.
- **Curriculum Learning (Tab. 4 Ours):** Training proceeds in three stages of 3,000 episodes each: (1) only easy motions $MDS < 200$, (2) easy + medium motions $MDS < 300$, and (3) all motions (full dataset).

We evaluate both models using standard metrics established in PHC: root-relative mean per-joint position error (MPJPE-L), global MPJPE (MPJPE-G), acceleration distance (Acc-Dist), and velocity distance (Vel-Dist). Lower values indicate better performance. As shown in Table 4, the curriculum guided by MDS consistently outperforms the baseline across *all* metrics on the overall test set. Moreover, performance improvements are observed across all difficulty subgroups. We attribute this gain to the difficulty-aware progressive learning schedule enabled by MDS. These results highlight the practical value of our MDS benchmark in guiding the training of humanoid control policies.

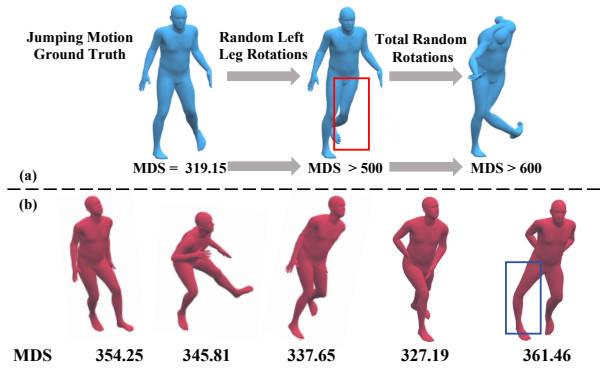


Figure 8. Illustration of the flawed motion detection potential.

(a) As an increasing number of joints in an originally natural motion are replaced with random, physically implausible rotations (i.e., introducing “flawed” poses), the MDS score rises dramatically. (b) On real noisy mocap data, visibly flawed motions (e.g., globally unbalanced or locally unnatural poses) exhibit substantially higher MDS values. Samples are picked from an inertial-sensor-based dataset [50].

C.2. Generalization to Other Humanoid Robots

In the main experiments, we follow the common practice of UHC [26] and PHC [24] by adopting an SMPL-based humanoid model as the controlled robot. However, given the structural similarity among humanoid robots, motions identified as challenging for the SMPL-based morphology are likely to pose comparable difficulties for other humanoid robots, suggesting strong generalization potential of our difficulty metric across different humanoid robots. In this section, we provide a preliminary demonstration of this generalization capability. We retarget motions of increasing difficulty (originally evaluated on the SMPL model) to the Unitree G1 [43] robot and qualitatively assess the imitation performance using the state-of-the-art G1-based controller TWIST [53]. As shown in Fig. 7, on relatively easy motions (left three columns), the policy reproduces the reference motion with minimal error; As MDS increases, noticeable failures emerge, such as incomplete leg rotation during turning (fourth column left), insufficient kick height (third column right), and, in the most challenging dance sequence (first column right), near-complete paralysis of both legs. The results reveal a consistent trend: imitation quality systematically degrades as MDS increases, confirming that the motion difficulty measured by our method on SMPL-structured data reliably generalizes to the G1 robot.

Furthermore, since our method is grounded in rigid-body dynamics, the proposed MDS is, in principle, applicable to other humanoid robotics and even systems beyond humanoid morphologies. We believe that further exploration of our benchmark on a broader range of robotic systems opens substantial and exciting avenues for future research.

C.3. Flawed Motion Detection

Motion capture (mocap) data frequently suffer from mocap inaccuracy and environmental interference, resulting in physically implausible or noisy motions that adversely affect downstream applications. Such artifacts are particularly pronounced in IMU-based motion capture systems due to sensor noise and calibration errors [18, 39, 58].

In this section, we conduct a simple yet illustrative experiment to demonstrate that our proposed MDS assigns markedly higher difficulty scores to unrealistic motions, thereby revealing its potential as an effective detector of such anomalies. We first demonstrate the behavior of MDS on “flawed” motions. For a natural jumping sequence (Fig. 8 (a), left), MDS yields a score of 319. When the four joints of the left leg are perturbed with random rotations (Fig. 8 (a), middle), the score exceeds 500. Further corrupting additional joints with physically implausible random rotations pushes MDS beyond 600 (Fig. 8 (a), right). These results provide clear evidence that unrealistic motions are consistently assigned substantially higher difficulty. Leveraging this property, we manually select several visually anomalous sequences from a representative IMU-based mocap dataset [50] (Fig. 8 (b)). Unstable and unbalanced motions (Fig. 8 (b), left four examples) exhibit significantly elevated MDS values, while sequences containing unnatural limb contortions (Fig. 8 (b), right) yield scores exceeding 360. The consistently high difficulty assigned to such defective motions underscores the potential of MDS as a principled and automated tool for flawed motion detection.